Available online at www.sciencedirect.com

SciVerse ScienceDirect

Procedia Computer Science 18 (2013) 1555 – 1563

Procedia Computer Science

2013 International Conference on Computational Science

# High-accuracy adaptive simulations of a Petri dish exposed to electromagnetic radiation

I. Gomez-Revuelto[a], L. E. García-Castillo[b], D. Pardo[c,d]

[a]*Departamento de Ingeniería Audiovisual y Comunicaciones. Universidad Politécnica de Madrid, Madrid, Spain.*
[b]*Departamento de Teoría de la Señal y Comunicaciones. Universidad Carlos III de Madrid.*
[c]*Department of Applied Mathematics, Statistics, and Operational Research, University of the Basque Country (UPV/EHU), Leioa, Spain.*
[d]*IKERBASQUE, Basque Foundation for Science, Bilbao, Spain.*

**Abstract**

This paper analyses numerically the electric field distribution of a liquid contained in a Petri dish when exposed to electromagnetic waves excited in a rectangular waveguide. Solutions exhibit high-gradients due to the presence of the dielectric liquid contained in the dish. Furthermore, electromagnetic fields within the dielectric have a dramatically lower value than on the remaining part of the domain, which difficults its simulation. Additionally, various singularities of different intensity appear along the boundary of the Petri dish. To properly reproduce and numerically study those effects, we employ a highly-accurate *hp*-adaptive finite element method. Results of this study demonstrate that the electric field generated within the circular Petri dish is non-homogeneous, and thus, a better shape, size, or location of the dish is needed to achieve an equally distributed radiation enabling the uniform growth of cell cultives.


Selection and peer review under responsibility of the organizers of the 2013 International Conference on Computational Science

*Keywords:* Finite Element Method (FEM), hp-adaptivity, electromagnetism, Petri dish.

## 1. Introduction

Since the German bacteriologist Julius Richard Petri proposed the use of the so-called *Petri dish* in the year 1887, its use has been widely extended among biologists to control the growth of a variety of cell cultives (see, for example, [1, 2]). It is often the case that the liquid contained within the dish is exposed to an artificial electromagnetic radiation that produces a source of heat, thus, facilitating and expediting the growth of the cell cultive. In multiple occasions, this radiation is attained by placing the dish within a waveguide that is electromagnetically excited through one of its ports. Ideally, the dish should be subject to a homogeneous electromagnetic field distribution, although in practice, this objective is rarely achieved.

In here, we study in detail via numerical simulations the spatial electrical distribution within the Petri dish resulting from its exposition to electromagnetic radiation in a rectangular waveguide. We consider the geometry depicted in Figure 1. Since our model problem is symmetric, in addition to the full problem, we shall also model

*The work reported in this paper was funded by the Spanish Ministry of Science and Innovation under the projects TEC2010-18175/TCM and MTM2010-16511.
**E-mail address*: dzubiaur@gmail.com (David Pardo).


Selection and peer review under responsibility of the organizers of the 2013 International Conference on Computational Science
doi:10.1016/j.procs.2013.05.323

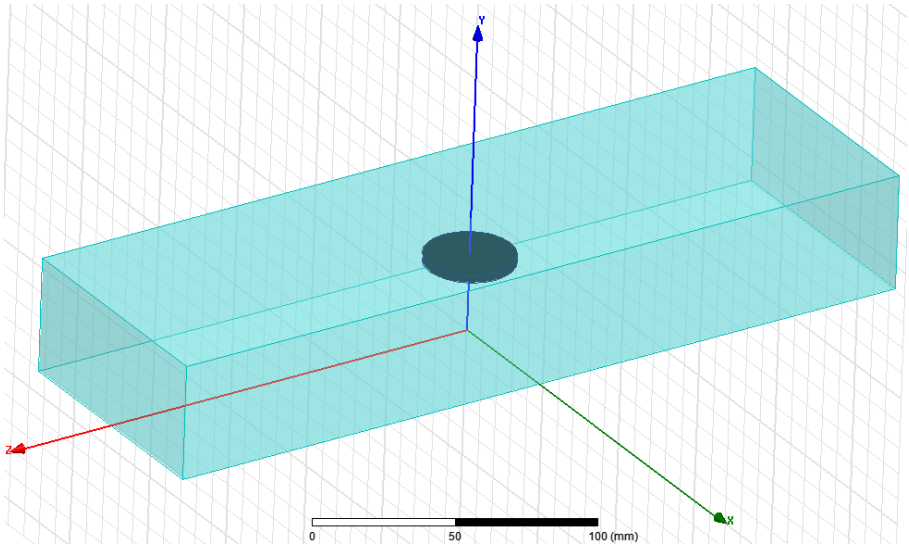


Figure 1. Geometry of a Petri dish of 0.0169 m radius and height equal to 0.003 m embedded in a rectangular waveguide of size 0.095 m x 0.045 m x 0.300 m.

half of the problem equipped with symmetry boundary conditions.

A preliminary numerical study of a Petri dish exposed to electromagnetic radiation can be found in [3]. In here, we employ a more accurate numerical method based on a three-dimensional (3D) fully automatic *hp*-adaptive FEM that enables a more accurate description of the resulting electromagnetic fields within the dish. This method combines the geometrical flexibility of a FEM with an accuracy that is superior to that provided by other numerical (and often even semi-analytical) methods. The resulting meshes delivered automatically by the *hp*-adaptive strategy adapt to the problem of interest. This grid-refinement strategy efficiently deals with different types of singularities appearing in the simulation of the Petri dish problem. Moreover, the dispersion (pollution) error is also automatically minimized by increasing the polynomial order of approximation, and therefore, the method is also suitable for efficiently solving the problem at a high-frequency regime.

This study serves as an initial design step towards optimizing the shape, size, number, and/or location of a Petri dish in order to homogenize the spatial distribution of the electric field within the dish. Additionally, it also illustrates the performance of the *hp*-adaptive strategy in real-life three-dimensional problems that simultaneously exhibit multiple singularities and high-gradients in the solution.

In the following, we derive the variational formulation, we introduce the numerical method, and we show the main results of our extensive numerical experimentation.

## 2. Mathematical Formulation

For a nonzero time-harmonic excitation ($\omega \neq 0$) in the frequency domain, our problem is governed by Ampére and Faraday's laws, given by:

$$\begin{aligned} \nabla \times \mathbf{E} &= -j\omega\mu\mathbf{H} && \text{(Faraday's law)}, \\ \nabla \times \mathbf{H} &= (j\omega\varepsilon + \sigma)\mathbf{E} + \mathbf{J}^{imp} && \text{(Ampére's law)}, \end{aligned}$$

where $\mathbf{E}$ and $\mathbf{H}$ are the electric and magnetic field, respectively, $j = \sqrt{-1}$ is the imaginary unit, $\mathbf{J}^{imp}$ is the impressed volumetric electric current, $\sigma$ is the conductivity of the media, and $\epsilon$ and $\mu$ are the electric permittivity and magnetic permeability of the medium, respectively. By convention, we express $\epsilon = \epsilon_r\epsilon_0$ and $\mu = \mu_r\mu_0$, where the 0-subscript denotes the material properties in vacuum, and the $r$-subscript indicates the relative factor in the actual material. In the application considered in this paper, both $\mathbf{J}^{imp}$ and $\sigma$ are equal to zero, $\epsilon_r$ is equal to 77 within the Petri dish and 1 in the remaining part of the domain, and $\mu_r$ is equal to 1 everywhere. The frequency of

operation is $f = \omega/(2 * pi) = 2.368$ GHz. The excitation of the problem is imposed via a boundary condition at the incident port, namely:

$$\hat{\mathbf{n}} \times \frac{1}{\varepsilon}\nabla \times \mathbf{H} + j\frac{\omega^2\mu}{\beta_{10}}\hat{\mathbf{n}} \times \hat{\mathbf{n}} \times \mathbf{H} = \mathbf{U}^{\text{in}} \text{ at the port boundary } (\Gamma_{in}) \tag{1}$$

where $\hat{\mathbf{n}}$ is the unit vector normal (and outward) to $\Gamma$, $\beta_{10}$ is equal to $2\pi$ divided by the wavelength within the waveguide, and $\mathbf{U}^{\text{in}}$ is defined as

$$\mathbf{U}^{\text{in}} = j\frac{k^2}{\varepsilon\beta_{10}}\hat{\mathbf{n}} \times \hat{\mathbf{n}} \times \mathbf{H}^{\text{in}} \tag{2}$$

with $\mathbf{H}^{\text{in}}$ being the incident magnetic field at the port.

For the exit port $\Gamma_{ex}$, we employ the same condition with $\mathbf{H}^{\text{in}} = \mathbf{0}$, which becomes an absorbing boundary conditions for the considered example, where the only present mode with non-negligible amplitude at the exit port is the so-called $\text{TE}_{10}$ mode. The remaining modes are evanescent: their amplitude diminish exponentially as a function of the distance to the Petri dish. The waveguide walls are modeled via perfect electric boundary conditions:

$$\hat{\mathbf{n}} \times \frac{1}{\varepsilon}\nabla \times \mathbf{H} = \mathbf{0}, \qquad \text{at perfect electric conductors } (\Gamma_N) \tag{3}$$

The above system of two first order PDE's can be further simplified to a single second order PDE in terms of magnetic field $\mathbf{H}$ by taking the curl of Ampére's law pre-multiplied by $1/\epsilon$ and using Faraday's law to obtain the so called reduced wave equation:

$$\nabla \times \frac{1}{\varepsilon}\nabla \times \mathbf{H} - \omega^2\mu\mathbf{H} = \mathbf{0} \tag{4}$$

The standard variational formulation is obtained by multiplying (4) by a test function $\mathbf{F} \in \mathbf{H}(\text{curl}, \Omega) = \{\mathbf{F} \in \mathbf{L^2}(\Omega) : \nabla\times\mathbf{F} \in \mathbf{L^2}(\Omega)\}$, integrating by parts, and incorporating the boundary conditions to obtain:

$$\int (\nabla \times \mathbf{F}) \cdot (\frac{1}{\varepsilon}\nabla \times \mathbf{H})\, d\Omega - \omega^2 \int \mathbf{F} \cdot \mu\mathbf{H}\, d\Omega + j\frac{\omega^2\mu}{\beta_{10}} \int_{\Gamma_{in}\cup\Gamma_{ex}} (\hat{\mathbf{n}} \times \mathbf{F}) \cdot (\hat{\mathbf{n}} \times \mathbf{H})\, d\Gamma = 2j\frac{\omega^2\mu}{\beta_{10}} \int_{\Gamma_{in}} (\hat{\mathbf{n}} \times \mathbf{F}) \cdot (\hat{\mathbf{n}} \times \mathbf{H}^{\text{in}})\, d\Gamma. \tag{5}$$

The electric field is computed by postprocessing the magnetic field using Ampére's law. Alternatively, one could directly derive a similar variational formulation in terms of the electric field.

## 3. *hp* Finite Elements and Automatic Adaptivity

For the numerical simulations, we employ a three-dimensional *hp*-adaptive finite element method [4, 5], where both the element size $h$ and polynomial order of approximation $p$ vary locally throughout the grid. The optimal distribution of element size $h$ and polynomial order of approximation $p$ is decided based on a self-adaptive strategy devised in [6] and further improved in [7, 5, 8]. This strategy utilizes as one of its main building blocks the *projection based interpolation* operator [9, 10]. The main advantage of this method is that it provides exponential convergence in terms of the energy-norm error vs. the problem size (see [11, 12, 13, 14, 15, 16, 17]), while it also minimizes the dispersion error in wave propagation problems due to the use of high $p$ (see [18, 19, 20]).

## 4. Numerical Results

In order to evaluate the accuracy of the simulation results, we start by analyzing the convergence of the *hp*-adaptive finite element method. In waveguide simulations, it is customary to measure the so-called *scattering matrix* $S$, whose entries $S_{ij}$ indicate the amount of energy measured at port $j$ when the $i$-th port is excited [8]. Figure 2 displays the convergence history of $S_{11}$ and $S_{21}$ for the symmetric (using symmetry boundary conditions) and full models. Results for $S_{12}$ and $S_{22}$ are similar and omitted here for brevity. These graphics confirm the high-accuracy delivered by the adaptive method. After a quick initial descend of the error in the pre-asymptotic

regime, the method stabilizes in the asymptotic regime with an exponentially fast convergence, as indicated by the obtained straight lines in the displayed scale. The initial, one intermediate, and final *hp*-grids corresponding to the full and symmetric models are displayed in Figures 3 and 4, respectively. We observe different final grids for the symmetric and full models due to the extreme sensitivity of the refinement strategy to the initial grid, which is different for each model. Nevertheless, final *hp*-grids in both models exhibit similar trends. In particular, heavy *h*- and *p*- refinements appear in the proximity of the Petri dish, as physically expected due to the singular behavior of the electromagnetic fields in that area of the domain.

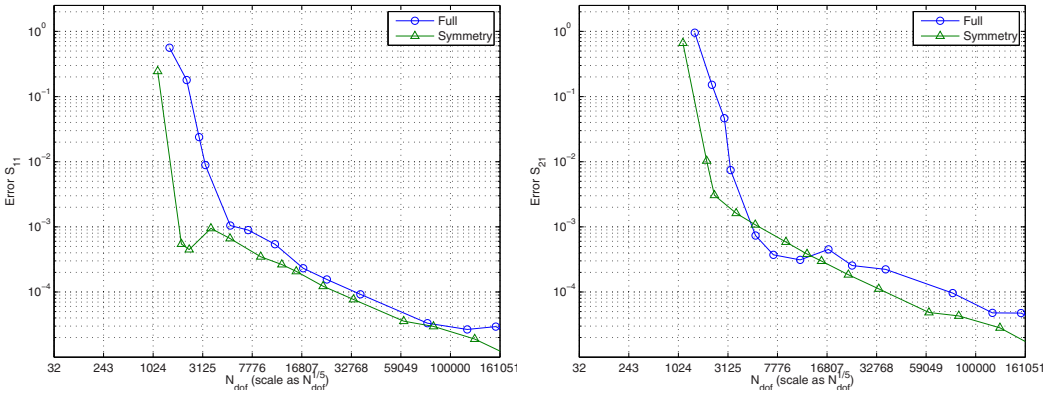


Figure 2. Petri dish embedded in a rectangular waveguide. Convergence history for the $S_{11}$ (left panel) and $S_{21}$-parameters (right panel). Errors (in absolute value) are estimated using a reference solution obtained from a globally refined *hp*-grid.

The energy distribution expressed in terms of $|E|^2$ $(V^2/m^2)$ over the Petri dish at different cut-off planes is displayed in Figure 5. We observe large variations on the electric field distribution along all spatial directions. This implies that the cell cultive will be subject to different heat levels, which is undesired. A more precise description of these undesired variations in the electric field can be observed in Figure 6, where we display some of its components. We conclude that the electric field experiments an abrupt variation (high gradients) around the dish boundary. This effect, is further observed in Figure 7, where we clearly visualize the singularities that develop at the corners of the Petri dish.

## 5. Discussion of Results and Conclusions

Results indicate that the electromagnetic fields rapidly vary in the proximity of the boundary of the Petri dish. Specifically, their amplitude significantly decrease within the dielectric dish. This low-intensity field also has important variations in both vertical and horizontal directions, which is an undesired situation for the proper growth of cell cultives. Thus, it is convenient to modify the shape and/or location of the Petri dish in order to recover a more homogeneous field distribution within the Petri dish.

The use of adaptive methods is necessary to accurately model the spatial distribution of the electric field within the Petri dish, since it is surrounded by a higher-energy field that contains singularities and high-gradients.

## References

## References

[1] E. Shirling, D. Gottlieb, Methods for characterization of streptomyces species, International Journal of Systematic Bacteriology 16 (3) (1966) 313–340.
[2] S. Zhang, Beyond the petri dish, Nature biotechnology 22 (2) (2004) 151–152.
[3] J. Varela, J. Page, J. Esteban, Design, implementation, and dosimetry analysis of an s-band waveguide in vitro system for the exposure of cell culture samples to pulsed fields, Bioelectromagnetics 31 (6) (2010) 479–487.

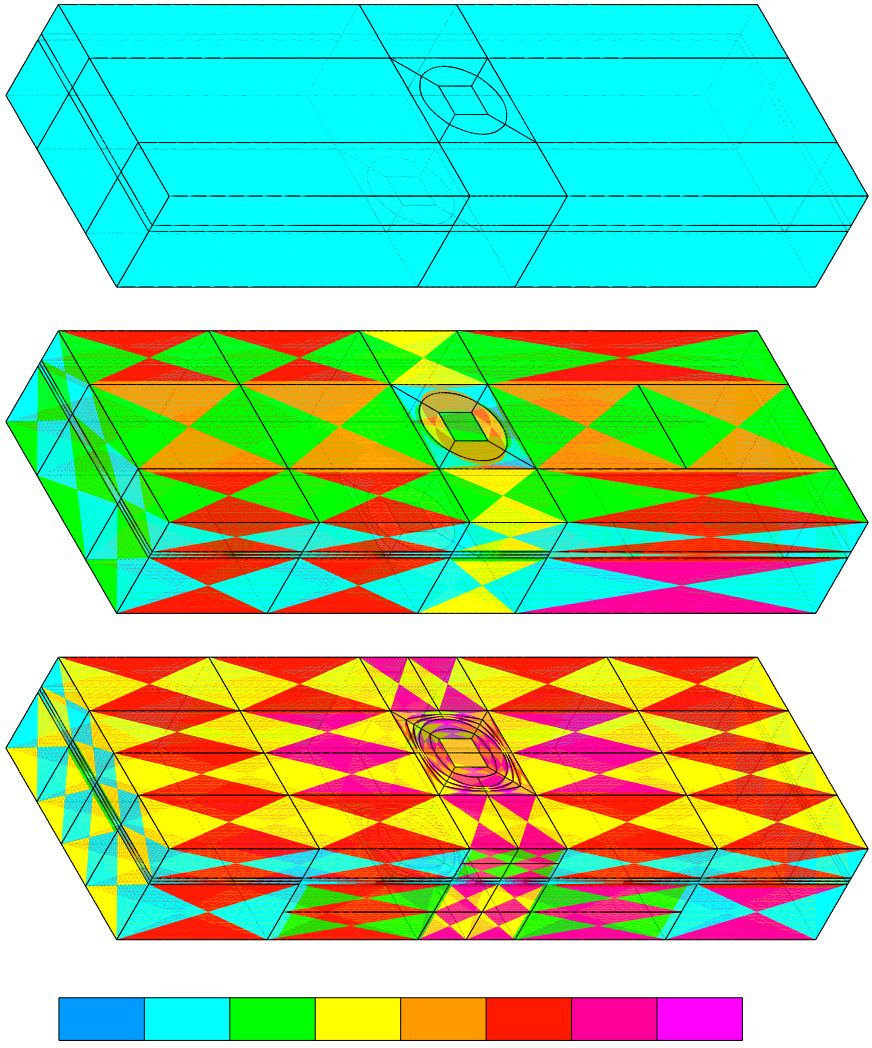

Figure 3. Petri dish embedded in a rectangular waveguide. Initial (top panel), intermediate (middle panel), and final (last panel) *hp*-grids delivered by the self-adaptive refinement strategy. Different colors indicate different polynomials orders of approximation, ranging from p=1 (dark blue) to p=8 (pink).


[4] L. Demkowicz, Computing with *hp* Finite Elements. I. One- and Two-Dimensional Elliptic and Maxwell Problems, Chapman & Hall/CRC Press, Taylor and Francis, 2007.

[5] L. Demkowicz, J. Kurtz, D. Pardo, M. Paszynski, W. Rachowicz, A. Zdunek, Computing with *hp* Finite Elements. II Frontiers: Three Dimensional Elliptic and Maxwell Problems with Applications, Chapman & Hall/CRC Press, Taylor and Francis, 2008.

[6] W. Rachowicz, D. Pardo, L. F. Demkowicz, Fully automatic *hp*-adaptivity in three dimensions, Computer Methods in Applied Mechanics and Engineering 195 (37-40) (2006) 4186–4842.

[7] J. Kurtz, L. F. Demkowicz, A fully automatic *hp*-adaptivity for elliptic PDEs in three dimensions, Computer Methods in Applied Mechanics and Engineering 196 (2007) 3534–3545, doi:10.1016/j.cma.2006.10.053.

[8] I. Gomez-Revuelto, S. Llorente-Romano, D. Pardo, et al., A three-dimensional self-adaptive *hp* finite element method for the characterization of waveguide discontinuities, Computer Methods in Applied Mechanics and Engineering 249-252 (2012) 62–74.

[9] L. F. Demkowicz, Encyclopedia of Computational Mechanics, John Wiley & Sons, Inc., 2004, Ch. "Finite Element Methods for Maxwell Equations".

[10] L. F. Demkowicz, A. Buffa, $H^1$, $H$(curl) and $H$(div)-conforming projection-based interpolation in three dimensions. Quasi optimal $p$-interpolation estimates, Computer Methods in Applied Mechanics and Engineering 194 (2–5) (2005) 267–296.

[11] W. Gui, I. Babuška, The $h$, $p$ and $h-p$ versions of the finite element method in 1 dimension - Part I. The error analysis of the $p$-version,

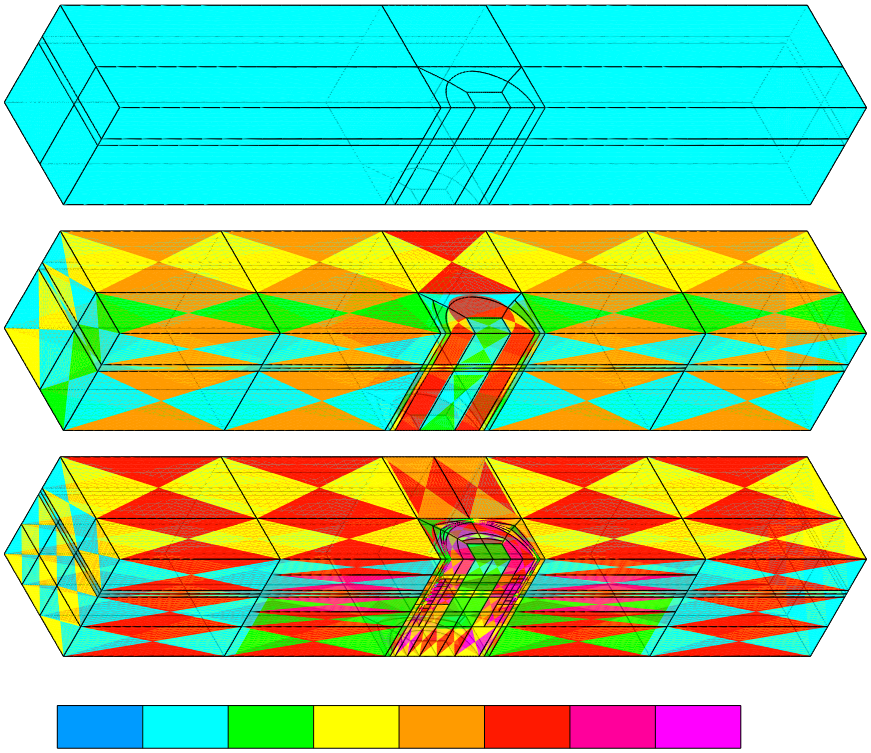

Figure 4. Petri dish embedded in a rectangular waveguide using symmetric boundary conditions. Initial (top panel), intermediate (middle panel), and final (last panel) $hp$-grids delivered by the self-adaptive refinement strategy. Different colors indicate different polynomials orders of approximation, ranging from p=1 (dark blue) to p=8 (pink).

Numerische Mathematik 49 (1986) 577–612.
[12] W. Gui, I. Babuška, The $h$, $p$ and $h-p$ versions of the finite element method in 1 dimension - Part II. The error analysis of the $h$- and $h-p$ versions, Numerische Mathematik 49 (1986) 613–657.
[13] W. Gui, I. Babuška, The $h$, $p$ and $h-p$ versions of the finite element method in 1 dimension - Part III. The adaptive $h-p$ version, Numerische Mathematik 49 (1986) 659–683.
[14] I. Babuška, B. Guo, Regularity of the solutions of elliptic problems with piecewise analytic data. Part I. Boundary value problems for linear elliptic equation of second order, SIAM Journal of Mathematical Analysis 19 (1) (1988) 172–203.
[15] I. Babuška, B. Guo, Regularity of the solution of elliptic problems with piecewise analytic data. II: The trace spaces and application to the boundary value problems with nonhomogeneous boundary conditions, SIAM Journal of Mathematical Analysis 20 (4) (1989) 763–781.
[16] I. Babuška, B. Guo, Approximation properties of the $hp$-version of the finite element method, Computer Methods in Applied Mechanics and Engineering 133 (1996) 319–346.
[17] C. Schwab, $p$- and $hp$- Finite Element Methods. Theory and Applications in Solid and Fluid Mechanics, Oxford University Press, 1998.
[18] F. Ihlenburg, I. Babuška, Finite element solution of the Helmholtz equation with high wave number. I: The $h$-version of the FEM, Computer and Mathematics with Applications 30 (9) (1995) 9–37.
[19] F. Ihlenburg, I. Babuška, Dispersion analysis and error estimation of Galerkin finite element methods for Helmhotz equation, International Journal for Numerical Methods in Engineering 38 (1995) 3745–3774.
[20] F. Ihlenburg, I. Babuška, Finite element solution of the Helmholtz equation with high wave number. II: The $h-p$-version of the FEM, SIAM Journal of Numerical Analysis 34 (1) (1997) 315–358.

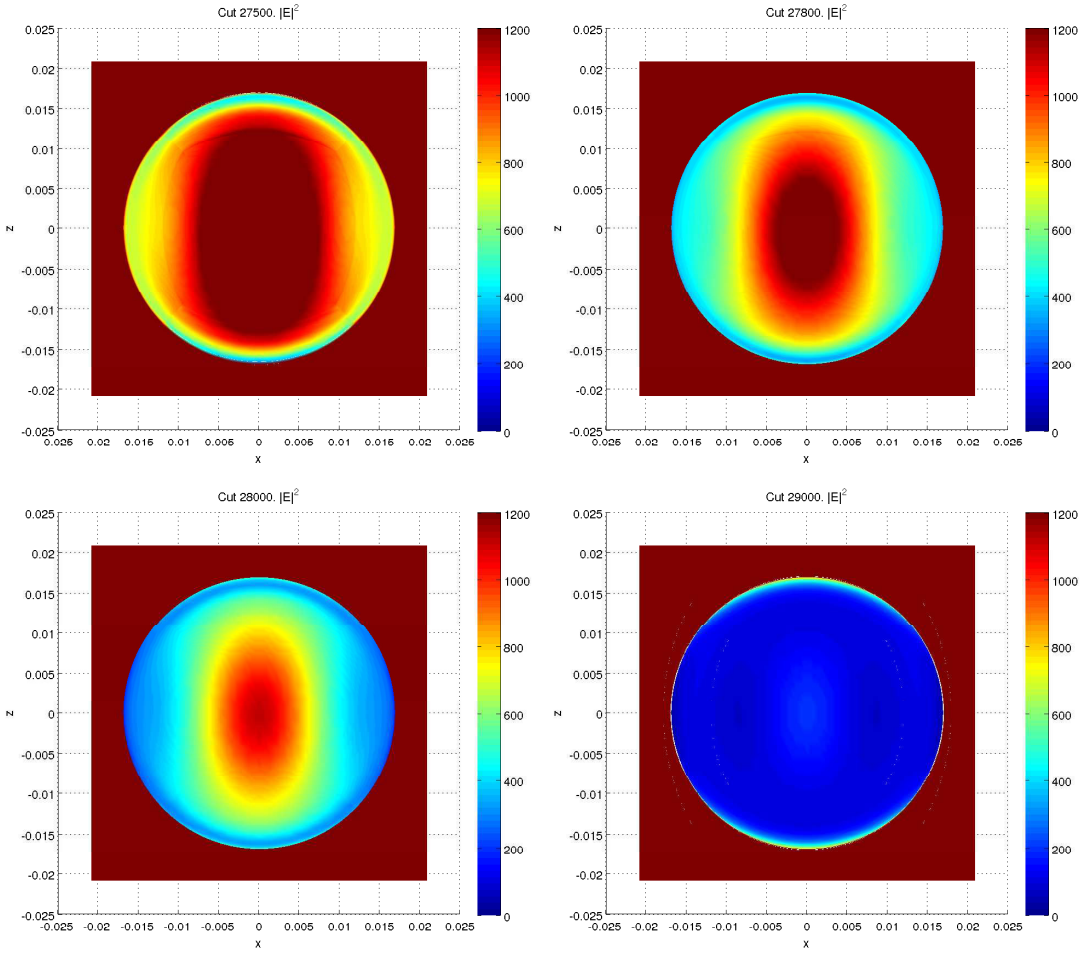


Figure 5. Energy distribution expressed as $|\mathbf{E}|^2$ $(V^2/m^2)$ over the Petri dish at different cut-off planes.

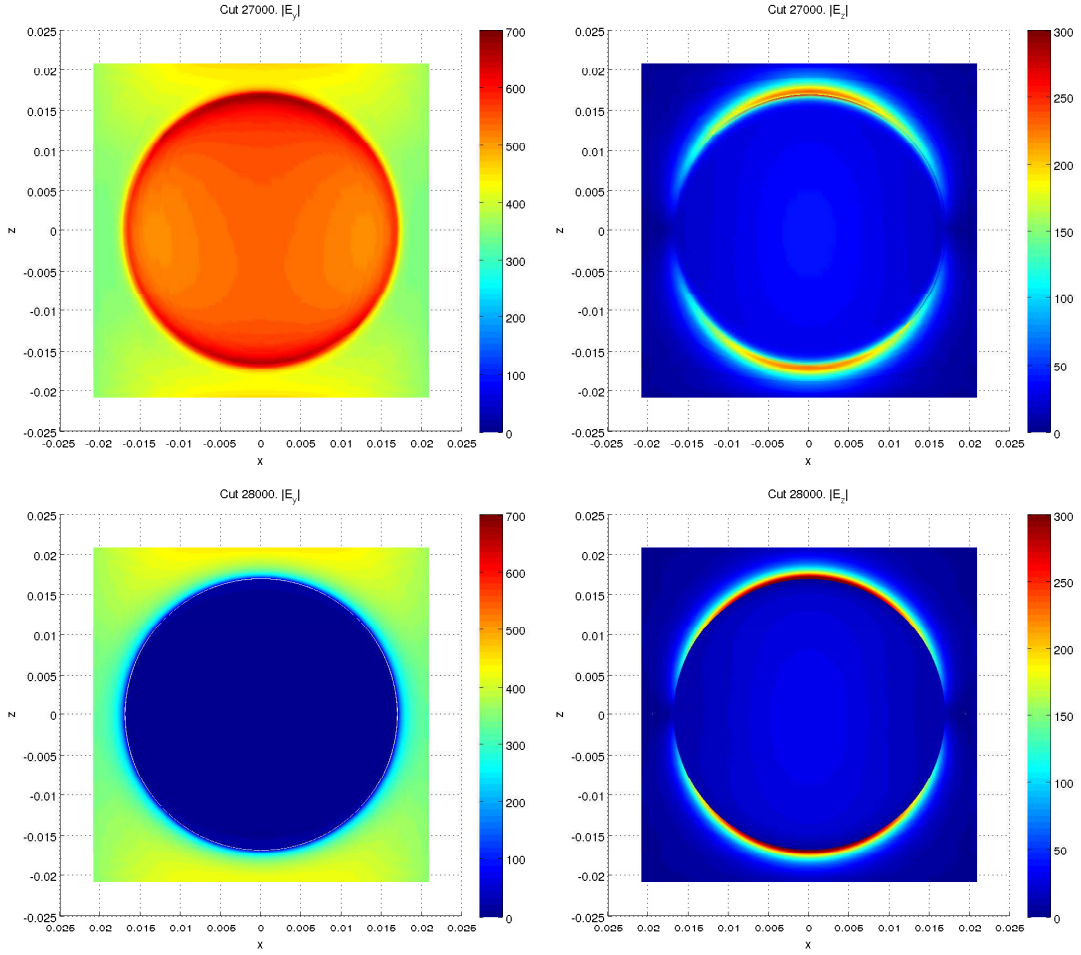


Figure 6. Absolute value of the $y$ and $z$ components of the electric field ($V/m$) over the Petri dish at different cut-off planes.

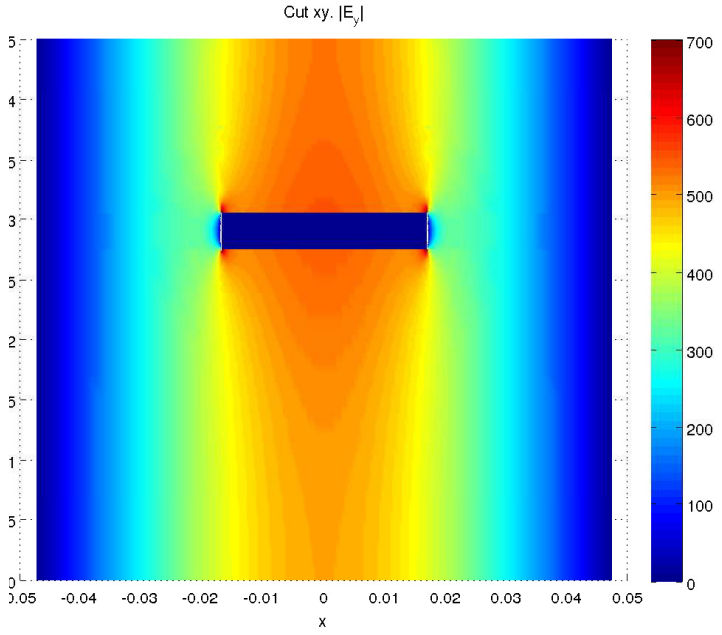


Figure 7. Absolute value of $E_y(V/m)$ across the $xy$ plane that cuts the Petri dish in half.